Singular characteristics and unique chemical bond activation mechanisms of photocatalytic reactions on plasmonic nanostructures

Phillip Christopher[1,2,3], Hongliang Xin[1], Andiappan Marimuthu[1] and Suljo Linic[1]*

The field of heterogeneous photocatalysis has almost exclusively focused on semiconductor photocatalysts. Herein, we show that plasmonic metallic nanostructures represent a new family of photocatalysts. We demonstrate that these photocatalysts exhibit fundamentally different behaviour compared with semiconductors. First, we show that photocatalytic reaction rates on excited plasmonic metallic nanostructures exhibit a super-linear power law dependence on light intensity (rate $\propto$ intensity^n, with $n > 1$), at significantly lower intensity than required for super-linear behaviour on extended metal surfaces. We also demonstrate that, in sharp contrast to semiconductor photocatalysts, photocatalytic quantum efficiencies on plasmonic metallic nanostructures increase with light intensity and operating temperature. These unique characteristics of plasmonic metallic nanostructures suggest that this new family of photocatalysts could prove useful for many heterogeneous catalytic processes that cannot be activated using conventional thermal processes on metals or photocatalytic processes on semiconductors.

Ever since the reports by Fujishima and Honda that TiO_2 illuminated with ultraviolet radiation could split water, the field of heterogeneous photocatalysis has almost exclusively focused on semiconductors[1–3]. There have been many efforts to address inherent deficiencies associated with the performance of most semiconductors, including attempts to: engineer the band gap to match the solar spectrum[4], improve catalytic activity by adding co-catalysts[2,5], and localize energetic charge carriers at the sites where photocatalytic transformations take place (that is, the surface of the semiconductor) by adding sensitizers[6,7]. It has also been recognized that the diffuse nature of the solar flux and the negative dependence of photocatalytic rates on operating temperature represent critical obstacles resulting in low rates of photocatalytic reactions per material volume (mass) even for relatively efficient semiconductors[8,9].

We demonstrated recently that plasmonic metallic nanostructures with engineered optical and catalytic properties also activate steady-state photocatalytic reactions under low-intensity visible light illumination[10]. In this Article we show that direct photocatalytic transformations on plasmonic metallic nanostructures are singular in several respects, and that this new family of photocatalysts exhibits fundamentally different behaviour compared with semiconductors. First, we observe that the rates of photocatalytic reactions on excited plasmonic metallic nanostructures show a super-linear power law dependence on light intensity (that is, rate $\propto$ intensity^n, with $n > 1$), at intensities $\sim 10^9$ times lower than the intensities required for super-linear behaviour on extended metal surfaces[11]. As a result, photocatalytic reactions on plasmonic nanostructures are characterized by a positive relationship between quantum efficiency and photon flux. In general, semiconductors exhibit lower quantum efficiency at higher light intensity[12]. A second singular characteristic of photocatalytic

transformations on plasmonic metallic nanostructures is that the rate and quantum efficiency of photocatalytic reactions increase with operating temperature. Conventional semiconductor photocatalysts in general exhibit lower reaction rates at higher temperatures[8,13]. The observed positive dependence of quantum efficiency and photocatalytic reaction rate on light intensity and operating temperature shows that, unlike semiconductor photo-catalysts, plasmonic nanostructures effectively couple thermal and photonic stimuli to drive chemical transformations. We propose a molecular model, based on first-principles calculations, describing the mechanism of chemical transformations on excited plasmonic nanostructures. Although this model supports our experimental findings, we also discuss other mechanisms that could potentially explain the observed behaviour.

We use catalytic partial oxidation of ethylene to form ethylene oxide (ethylene epoxidation, $C_2H_4 + 1/2O_2 \rightarrow C_2H_4O$) as the model reaction[14]. Reactor studies were carried out in a vertically oriented packed-bed reactor filled with a 20% wt loading of 75 nm edge length plasmonic Ag nanocubes supported on inert α-Al_2O_3 particles. See Methods for details. We have shown previously that under these operating conditions the steady-state reaction rate is controlled by the rate of O_2 dissociation[10], that is, we essentially measure the steady-state rate of O_2 dissociation on plasmonic Ag nanostructures as a function of temperature and illumination intensity at constant atmospheric pressure. The photocatalytic reaction rate at a given temperature was obtained by subtracting the rate of the pure thermal process (light off) from the rate of the photo-thermal process (light on).

Figure 1a shows a scanning electron micrograph of the photocatalyst, which contains isolated and clustered Ag nanocubes, separated by larger Al_2O_3 alumina particles. The diffuse reflectance ultraviolet–visible extinction spectrum in Fig. 1b shows a large

[1]Department of Chemical Engineering, University of Michigan, Ann Arbor, Michigan 48109, USA, [2]Department of Chemical and Environmental Engineering, University of California, Riverside Riverside, California 92521, USA, [3]Program in Materials Science and Engineering, University of California, Riverside Riverside, California 92521, USA. *e-mail: linic@umich.edu.
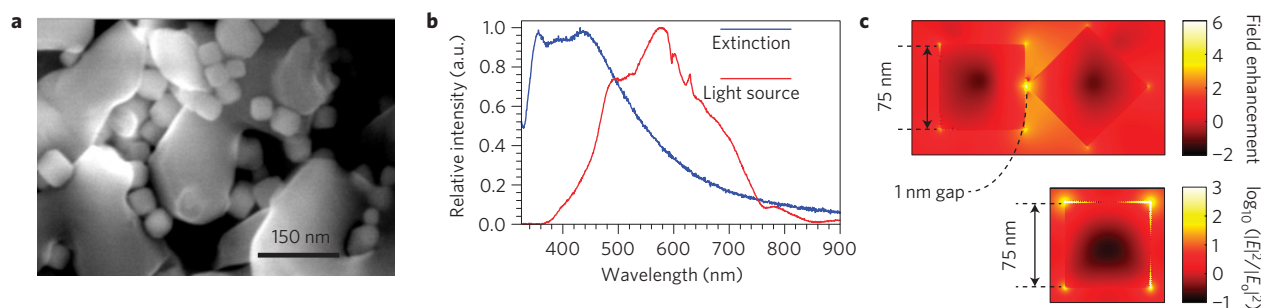
Figure 1 | Geometric and optical characteristics of plasmonic photocatalyst. a, Scanning electron micrograph of the catalyst containing densely packed Ag nanocubes supported on α-Al$_2$O$_3$. **b**, Diffuse reflectance ultraviolet–visible extinction spectrum of Ag nanocubes on α-Al$_2$O$_3$. The emission spectrum of the visible light source is also shown. **c**, Calculated spatial distribution of the electric field intensity for two 75 nm edge length Ag nanocubes separated by 1 nm and an isolated 75 nm edge length Ag nanocube, at their respective resonant wavelengths (500 and 400 nm). The calculations were performed using the FDTD method (see Supplementary Information).

extinction of visible photons by the Ag nanostructures. The extinction is the consequence of the resonant excitation of localized surface plasmons. Localized surface plasmon resonance (LSPR) is characterized by intense, spatially non-homogeneous, oscillating electromagnetic fields in the neighbourhood of the nanostructures[15–17]. The local field intensity is dependent on the geometry of the nanostructure and the surrounding environment. For example, finite difference time domain (FDTD) simulations in Fig. 1c show that, under resonant photon excitation, the intensity of electric fields at the surface of an isolated particle is $\sim$10^3 times larger than the field intensity of the incoming photon flux. For two particles separated by $\sim$1 nm the field intensity enhancement is more than $\sim$10^6 (ref. 18). The excitation of LSPR is accompanied by a number of photo-physical processes, including intense scattering of resonant photons and high concentrations of energetic electrons at the surface of the plasmonic nanostructures[19]. This strong LSPR-mediated interaction of resonant light with plasmonic metal nanostructures has previously been exploited in many applications, including targeted cancer therapy[20], single-molecule spectroscopy[21] and fluorescence[22], surface-enhanced spectroscopy[23], among others. Herein, we show that this strong light–matter interaction can also drive catalytic reactions directly on plasmonic nanostructures.

Figure 2a shows the steady-state rate of photocatalytic ethylene epoxidation (limited by the dissociation of O$_2$) as a function of source intensity at different temperatures. We note that we established that the LSPR was responsible for the observed photocatalytic activity by showing that there was one-to-one mapping between the wavelength-dependent photocatalytic rate and the LSPR extinction spectrum (Supplementary Fig. S1). The figure shows that the photocatalytic rate exhibits a linear dependence on intensity up to $\sim$300 mW cm^{-2} and a super-linear, power-law dependence above $\sim$300 mW cm^{-2} (that is, rate $\propto$ intensity^n, with $n > 1$). The magnitude of the power law exponent reached a value of $n \sim 3.5$ at an intensity of $\sim$920 mW cm^{-2}. The transition was previously observed for photo-induced reactions on extended single-crystal metal surfaces at light intensities $\sim$10^9 times higher than the intensity in Fig. 2 (ref. 11). The observed intensity-dependent transition from the linear to super-linear regime is a signature of electron-driven chemical reactions on metals[11]. This is discussed in more detail later in this text.

Figure 2b shows the magnitude of the kinetic isotope effect (KIE), the ratio of steady-state rate of the photocatalytic process for the O$_2^{16}$ and O$_2^{18}$ isotopes, as a function of light intensity, measured at constant reaction rates. The steady-state reaction rate was controlled by manipulating the operating temperature between 408 and 498 K. The figure shows that at zero intensity (light off), the KIE (at $T = 498$ K) was $1.09 \pm .04$. This is consistent with O$_2$ dissociation controlling the rate of the reaction[10,24]. The KIE for

the thermal process (light off) changes by less than 1% for the range of temperatures, between 400 and 500 K, explored in these studies. Figure 2b shows that, in the linear rate-intensity regime (light intensity below 300 mW cm^{-2}), the KIE is $\sim$1.16 $\pm$ 0.04. Figure 2b also shows that when the reaction rate enters the super-linear regime, the KIE increases further, reaching 1.49 ± 0.09 at an intensity of 800 mW cm^{-2}. The enhanced KIE is a distinct signature of electron-driven photocatalytic reactions on metals[25]. The large KIE also indicates that light-induced local heating of the plasmonic nanostructures cannot account for the observed photocatalytic activity, consistent with our previous analysis of heating effects in these systems[10].

The results in Fig. 2c illustrate another singular characteristic of photocatalytic transformations on excited plasmonic metallic nanostructures: a positive relationship between operating temperature and the photocatalytic rate. The figure shows that at a constant light intensity, an increase in operating temperature resulted in an exponential increase in the photocatalytic reaction rate. The positive effects of light intensity (Fig. 2a) and temperature (Fig. 2c) on the rate of the photocatalytic process have dramatic consequences on the process quantum efficiency. Figure 2d shows the measured quantum efficiency as a function of source intensity for various temperatures. Quantum efficiency was calculated as the photocatalytic reaction rate divided by the rate of photons impinging on the catalyst bed (this quantity should not be confused with the thermodynamic efficiency). The figure shows that, at a constant temperature, the transition to the super-linear regime is accompanied by an increase in quantum efficiency. Furthermore, at a given source intensity, a higher operating temperature results in a higher quantum efficiency. As a result, the quantum efficiencies measured at elevated temperatures and high light intensities are very high[26,27]. For example, at a source intensity of 400 mW cm^{-2} and 473 K the quantum efficiency was $\sim$60%.

The experimental results in Fig. 2 lead us to suggest a possible mechanism for the LSPR-mediated reactions on metals. We propose that surface plasmons, formed in the process of optical excitation of Ag nanoparticles, relax by transferring electron density to O$_2$, thereby inducing electron-driven O$_2$ dissociation on Ag in both the linear and super-linear rate regimes. The results raise two critical questions related to the mechanism responsible for the transition from linear to super-linear intensity-rate behaviour and the nature of photocatalytically active sites.

In the framework of the proposed mechanism, Ag surface plasmons can transfer electron density to O$_2$ either directly through chemical interface damping or indirectly through the decay of plasmons into energetic e$^-$/h$^+$ and subsequent transfer of the e$^-$ to O$_2$ (ref. 15). Irrespective of the mechanism, energetic electrons can transiently populate unoccupied states (orbitals) of adsorbed
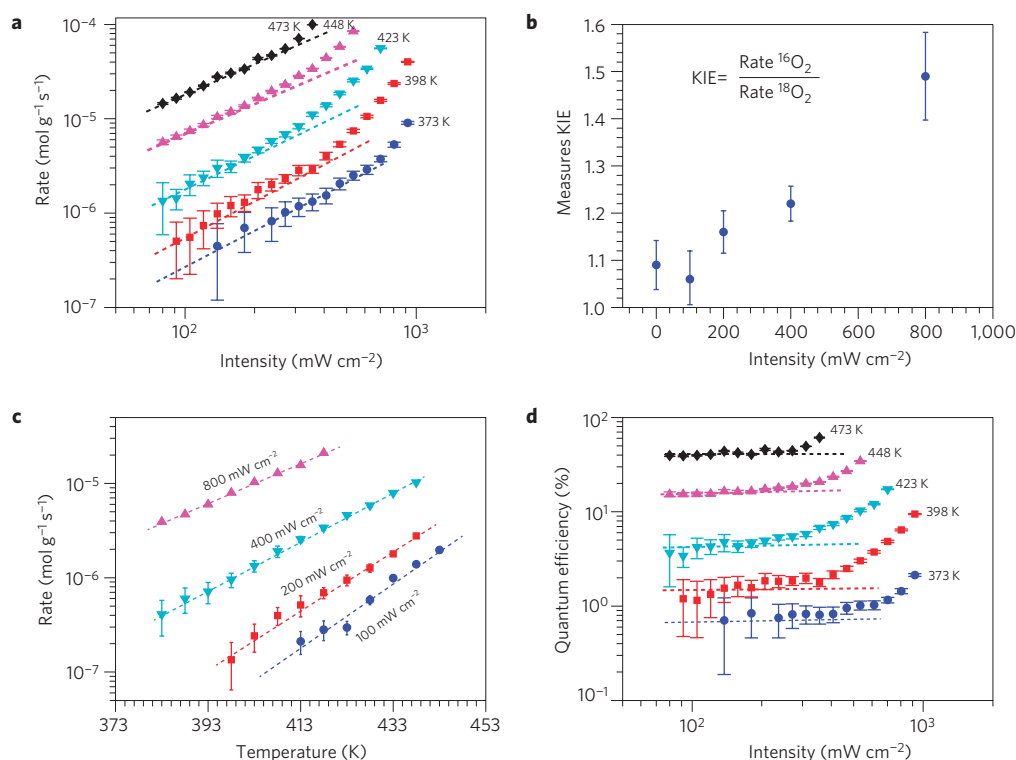
Figure 2 | Reaction rate, quantum efficiency and KIE as a function of intensity and temperature. a, photocatalytic rate as a function of light intensity for various temperatures. The dotted lines show the linear trend observed at source intensities $<\sim 300$ mW cm^{-2}. A super-linear dependence of rate on the intensity is observed at higher intensities. **b**, KIE, measured at constant reaction rate, as a function of source intensity. **c**, photocatalytic rate (log scale) as a function of operating temperature for various source intensities. **d**, Quantum efficiency (%) as a function of intensity for various temperatures. The dotted lines show the quantum efficiency observed at source intensities $<\sim 300$ mW cm^{-2}. Deviations from the linear trend are observed at higher intensities. Error bars represent standard deviation in the measurement over a 15 min sampling period.

O_2, inducing electron-mediated O_2 dissociation[15]. To analyse this process, we employed a molecular model to calculate the rate of electron-driven O_2 dissociation on the Ag(100) surface as a function of temperature and electron flux through the antibonding O–O orbital. The model is a modified version of models used previously to describe desorption induced by electronic transition (DIET) and desorption induced by multiple electronic transitions (DIMET) on metals[28,29].

The central feature of the model is that energetic electrons (formed on Ag in response to LSPR) populate unoccupied adsorbate orbitals (in this case the $2\pi^*$ antibonding O–O orbital) creating the transient negative ion (TNI) O_2^- species[10,30,31]. The TNI evolves on its potential energy surface (PES). In this process, the O–O bond is elongated owing to a shorter equilibrium bond distance for the neutral O_2 molecule than for the TNI (Supplementary Fig. S2). The TNI relaxes by releasing an electron back to the metal and returning to the neutral PES, albeit in an excited vibrational state. In this process the adsorbate acquires vibrational energy. It is assumed that the chemical reaction takes place when the vibrational energy is sufficient to overcome the activation barrier, see Fig. 3a. This assumption is reasonable, as the lifetime of excited vibrational states (a few picoseconds[32]) is significantly larger than the timescale of a vibration (a few femtoseconds[33])[34].

As discussed in the Supplementary Information, in the implementation of the model we employed a Newns–Anderson type Hamiltonian that included a non-adiabatic coupling of the energetic electron to adsorbate coordinate[35,36]. Density functional theory (DFT) calculations were used to calculate the PES of O_2 adsorbed on Ag(100) in its ground state. Linear expansion Δ-self consistent field-DFT was used to calculate the PES associated with the TNI (see Supplementary Fig. S2 for PES). We note that

the inherent inaccuracies associated with DFT calculations impact the quantitative value of the calculated reaction rate. However, a sensitivity analysis of the model, discussed in the Supplementary Information, showed that the model captures the underlying mechanisms and qualitative trends well, see Supplementary Figs S4 and S5.

Figure 3b shows the calculated reaction rate for the electron-induced dissociation of O_2 on the Ag(100) surface as a function of the frequency of scattering events between energetic electrons and the antibonding O–O orbital. The figure shows that the model captures the experimentally observed transition from a linear to super-linear dependence of the rate on electron flux. The model sheds light on the physical origin of the transition. In the linear regime, the molecule dissociates when a single electron scattering event deposits sufficient vibrational energy in the reaction coordinate. If the amount of energy deposited is insufficient to overcome the activation barrier, the adsorbate dissipates the excited vibrational energy, returning to the equilibrium thermal vibrational distribution before a subsequent scattering event. The transition to the super-linear regime occurs when the frequency of scattering events becomes sufficiently high (higher electron flux), such that the probability for electronic excitation of an adsorbate already vibrationally excited from previous electron scattering events becomes substantial (Fig. 3a; ref. 37). Not surprisingly, the model predicts that the transition to the super-linear reaction regime takes place when the scattering frequency is approximately equal to the inverse of the lifetime of the excited vibrational state of the adsorbate on a metal surface[38]. Assuming realistic lifetimes of $\sim 10^{-12}$–10^{-11} s, the critical scattering rate is between 10^{11} and 10^{12} s^{-1}.

The model also captures the experimentally observed increase of KIE with light intensity. Figure 3c shows a parity plot, comparing the experimentally measured KIE (from Fig. 2b) against the KIE
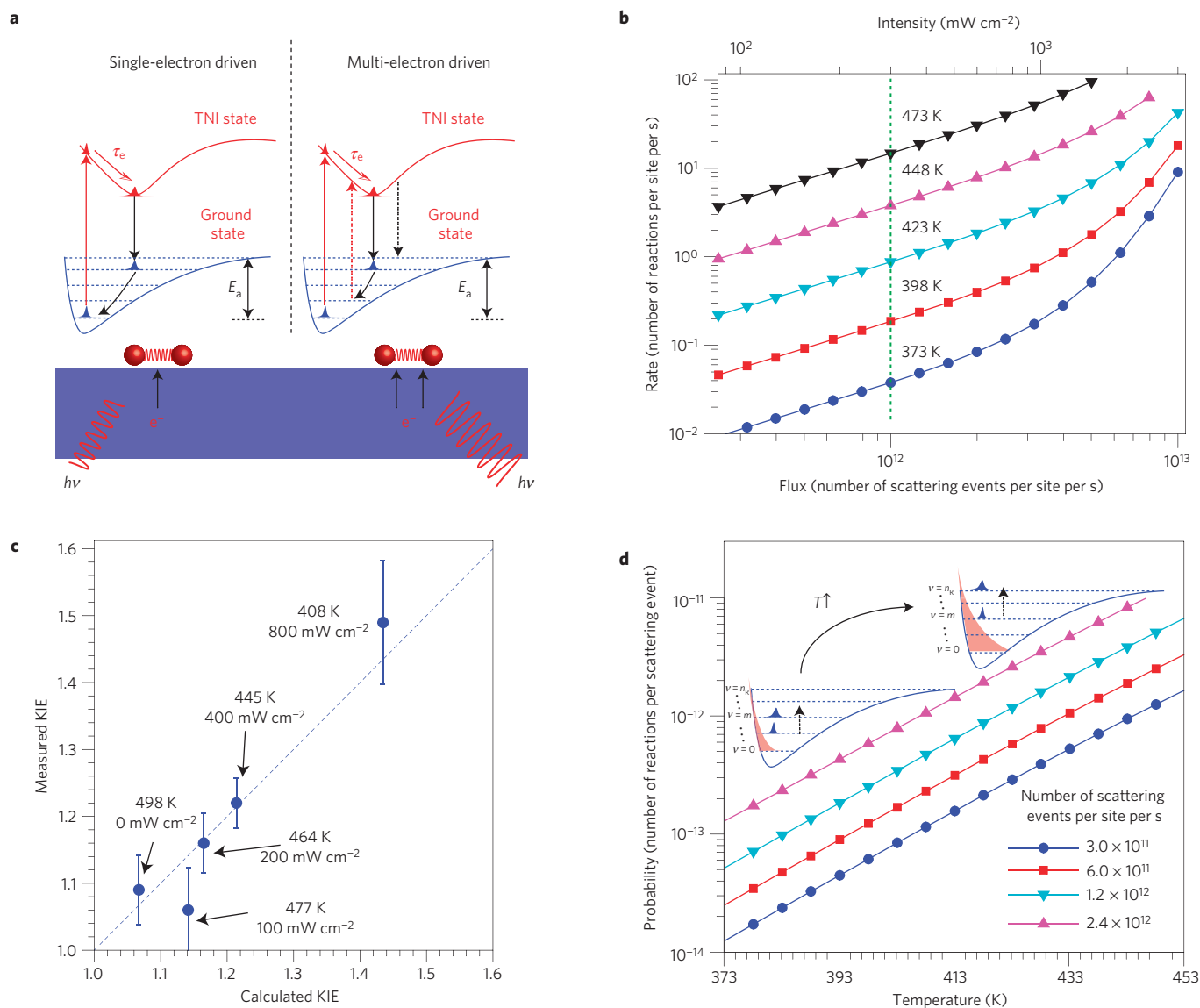
Figure 3 | Molecular model for electron-driven reactions on metals. a, The left panel shows the molecular mechanism in the linear regime. A single electron excitation deposits vibrational energy into the adsorbate by accelerating the molecule along the TNI PES for the lifetime, τ_e. If vibrational energy is not sufficient to overcome the activation barrier, E_a, the adsorbate returns to the thermally equilibrated state. The right panel shows that in the super-linear regime the adsorbate is electronically excited multiple times before overcoming the activation barrier. **b**, Simulated rate of O_2 dissociation as a function of the electron flux, analogous to the experimental results shown in Fig. 2a. The secondary x axis on top shows the experimental source intensity, related to the electron flux through a linear correlation by adjusting the point where the regime transition takes place. A vertical dashed line was used to denote such mapping. **c**, A parity plot of the experimentally measured and simulated KIE. The straight line indicates a complete agreement between measured and calculated KIE. **d**, The calculated reaction rate as a function of operating temperature for different intensities (correlated to the electron flux as described above and in the text). The plot is analogous to the experimental results in Fig. 2c. The inset shows a schematic of the effect of increasing temperature (higher occupancy of excited adsorbate vibrational states) on the gain of vibrational energy and, thus, the probability for the reaction.

obtained by calculating the rates of electron-induced dissociation of $O_2{}^{16}$ and $O_2{}^{18}$ on the Ag(100) surface using the model described above. The source intensity used in experiments and the electron flux used in the calculations were related to each other by linearly mapping the source intensity at which the transition to the super-linear rate takes place onto the electron-flux required for this transition. This mapping is illustrated through the secondary x axis on Fig. 3b. The difference in the rates of electron-driven dissociation of different O_2 isotopes is a consequence of different masses of oxygen atoms in the two isotopes. In classical terms, when subjected to an identical force on the TNI PES for the same lifetime the lighter isotope experiences greater acceleration, acquiring more vibrational energy, which results in a higher reaction probability.

In contrast, it has also been proposed that the larger KIE observed for electron-stimulated desorption of ionic species from a metal surface can be explained by the different lifetimes of the heavier and lighter isotopic ion in the neutralization region of the metal[39]. As the transition to the super-linear regime occurs, the KIE further increases because multiple scattering events result in a larger discrepancy in the vibrational energy gained by the two isotopes. The parity plot in Fig. 3c shows that there is a quantitative agreement between the experimentally measured and predicted KIE for the measurements performed in the linear and super-linear regimes. The quantitative agreement is not unexpected because, by comparing the two isotopes, inherent errors due to inaccuracies in DFT calculations are to a large degree cancelled.
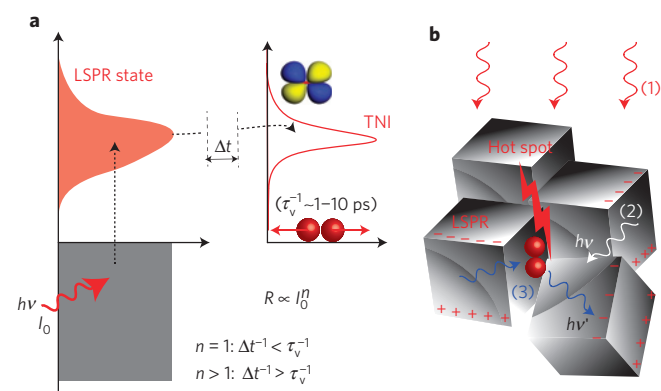
Figure 4 | Unique features of plasmonic photocatalysts. a, The schematic shows the plasmon-mediated electron transfer from Ag to the O_2 $2\pi^*$ orbital forming a TNI. When the rate of plasmon excitation, Δt^{-1}, is smaller than the vibrational decay rate of O_2, τ_v^{-1}, the photocatalytic rate is linear with respect to the source intensity. When $\Delta t^{-1} > \tau_v^{-1}$ the photocatalytic rate shifts to a super-linear dependence on source intensity. **b**, A schematic of the proposed active complex of plasmonic Ag particles that can support a super-linear rate is shown. Photons interacting with the active complex are: (1) from the source, (2) elastically scattered from other nanoparticles in the reactor or (3) inelastically scattered from the adsorbates. The super-linear rate is achieved at hot spots where the electromagnetic energy collected by the cluster is efficiently transferred to the adsorbate forming a TNI.

Figure 3d shows that the model also captures the experimentally observed exponential dependence of the photocatalytic rate on operating temperature at constant electron flux (light intensity). There are two critical mechanisms governing the temperature effect on the photocatalytic rate. First, at higher temperatures the relative population of adsorbate excited vibrational states increases according to the Bose–Einstein distribution. This means that, on average, the O_2 adsorbate will require less energy gain in electron scattering events to overcome the activation barrier. Second, it has been shown previously (also see Supplementary Fig. S3) that the probability of gaining a specific number of vibrational quanta increases when the molecule is initially in an excited vibrational state[35]. The two effects act to induce the observed exponential rate dependence on temperature, see the inset in Fig. 3d.

Figure 3 shows that all experimental observations can be accounted for by assuming that the photo-reaction takes place via electron scattering from Ag to the $2\pi^*$ state of adsorbed O_2. The proposed model suggests that the critical electron scattering frequency required for the transition from the single-electron process to the multi-electron process is 10^{11}–10^{12} scattering events per second. Assuming one-to-one mapping between the rate of plasmon formation and the electron scattering rate, it is difficult to see how a single Ag nanoparticle can supply enough plasmons (that is, energetic electrons) to support this process. The optical cross-section of large plasmonic Ag nano-cubes has been measured to be approximately twenty times larger than the geometric cross-section[40]. This means that, for a 75 nm cube and a source intensity of ~300 mW cm^{-2} of visible photons, the rate at which plasmons form is ~10^9 plasmons per particle per s, which is not sufficient to support the super-linear rate.

We postulate that active sites that support the super-linear rate are complexes of multiple Ag nanoparticles with the rate of plasmon formation on the complex larger than ~10^{11}–10^{12} plasmons per s, see Fig. 4a. The rate of plasmon formation in the active complex will depend on the local intensity of resonant photons impinging on the complex and the optical cross-section of the complex. In our three-dimensional (3D) reactor systems both quantities are spatially

variable. The local photon intensity can be enhanced by elastic scattering of resonant light by other Ag particles in the system. This elastic scattering effectively increases the photon path lengths in the reactor and therefore the steady-state photon intensity. Furthermore, when an inelastic scattering of plasmon energy to O_2 occurs, resulting in the formation of TNI, the relaxation of TNI species results in the emission of a new Stokes-shifted photon, which can excite another plasmon either on the reactive complex or somewhere else in the reactor. This process will be repeated until the multiply-Stokes-shifted photons exit the range of resonance at which they can excite plasmon states. Assuming a Stokes shift of one O_2 vibrational quanta (~0.1 eV) and a width of the LSPR of ~1 eV, we estimate that one photon can result in at least ten plasmons in the reactor. The combination of elastic and inelastic scattering of resonant and Stokes-shifted photons suggests that the local light intensity in sections of the 3D reactor can be significantly enhanced compared to the source light intensity; see Fig. 4b. As well as the variations in the local light intensity, the optical cross-section of the active complex can be very high, reaching values larger than 50 times the geometric cross-section[40]. We suggest that a combination of high local photon intensities and high optical cross-sections of particle complexes makes it feasible for the plasmon formation rate to reach the regime required for the transition to the super-linear rate regime on the complex.

Another requirement for the active complex is there has to be an efficient focusing of energy on some spots in the complex where plasmons decay, transferring electron density to O_2. Most probably, these spots are areas of the active complex where two particles (for example, edges of the cubes) are close to each other (on the order of 1 nm). In these junctions, the capacitive coupling of the oscillating electron cloud in one Ag particle—the oscillating of an electron cloud is a consequence of the resonant excitation of plasmon excitation—to the oscillating electron cloud of the neighbouring particle focuses the flux of charge carriers; that is, the concentration of energetic electrons is very high. It has been postulated that at these locations, the charge carriers can efficiently couple to the chemisorbed molecule, causing efficient charge transfer and the formation of TNI (ref. 41).

It is worth noting that a similar super-linear dependence of photo-yield on source intensity was observed in measurements of resonant surface enhanced Raman spectra of a dye molecule on two-dimensional clusters of large plasmonic Ag nanoparticles at source intensities between 3 and 300 W cm^{-2} (ref. 42). The molecular model that describes the resonant surface enhanced Raman spectra process is similar to the model discussed above for the photocatalytic reactions on plasmonic nanoparticles. Even in this earlier contribution, the unexpected super-linear behaviour was discussed in terms of 'active clusters' containing multiple Ag nanoparticles, which are efficient in resonant transfer of electrons to LUMO states of analyte molecules.

It is also important to state that other explanations for the observed super-linear rate-intensity behaviour are possible. It can be conceived that the interaction between energetic electrons and excited plasmons results in excitation and re-excitation of electrons, preventing their rapid thermalization and inducing a nonlinear response of non-thermalized electron density distribution to photon intensity. If this were the case, the nonlinear photo-yield would be observed even if the photo-reactions were driven by a single vibronic excitation[43,44]. It is hard to see how this mechanism can explain the observed dependence of KIE on the source intensity. Another possible mechanism, similar to a mechanism of chemical activation by local near fields discussed previously[45], involves the excitation of O_2 by inelastic collision of the molecule with the local plasmon-mediated electron density. The surface plasmons are characterized by high spatial and temporal gradients in electron density. It is possible for the O_2 molecule to interact with these

density gradients, gaining energy and moving to a higher energy (more reactive) state[45].

In conclusion, singular characteristics of photocatalytic transformations on plasmonic nanostructures include: a shift from a linear to a super-linear dependence of rate on source intensity, which was previously observed on metal single crystals only at $\sim 10^9$ times higher light intensities than those examined herein; a significantly larger intensity-dependent KIE compared to thermal processes; and an exponential dependence of the photocatalytic rate on the operating temperature. We demonstrate that, unlike most semiconductors, plasmonic metal nanostructures constructively couple the energy of photons and thermal energy with a reaction rate positively responding to both stimuli. We postulate that the 3D packing of Ag nanoaparticles in the reactor bed is critical for the observed transition from a linear to a super-linear dependence rate on intensity at relatively low photon intensities. We propose that the active sites responsible for this transition are clusters of closely packed plasmonic nanostructures.

Methods

Catalyst synthesis. Ag nanocubes were synthesized using a modified polyol process[10]. Briefly, 9 ml of highly pure ethylene glycol (J. T. Baker item 9300, lot # J43B13) was heated to 140 C. 100 μl of a 30 mM HCl in ethylene glycol solution was then injected into the heated ethylene glycol. After 10 min, 3 ml of 0.1 M AgNO₃ (99% purity, Sigma Aldrich cat. No. 209139) and 0.15 M PVP (55,000 M.W. Sigma Aldrich cat. No. 856568) were slowly, simultaneously injected into the EG and HCl solution. The mixture was allowed 24 h to nucleate single crystals seeds, open to the atmosphere. The vial was sealed and nanocubes formed over 2–3 h. The nanocubes were washed via five cycles of centrifugation and dispersal in ethanol. The nanocubes were then impregnated onto 0.1 g alpha-Al₂O₃ (Alfa Aesar, part number 10461).

Reactor experiments. The reactor set-up and catalyst synthesis have been previously described[10,46,47]. The catalyst was illuminated using a broadband visible light source with peak intensity at 590 nm, a minimum wavelength of 380 nm, and a variable intensity between 75 and 920 mW cm⁻². All rate measurements were performed in the light-limited regime. Therefore, the reported photocatalytic rates represent lower limits. The Ag nanocubes/Al₂O₃ catalyst was pretreated *in situ* based on previously reported methods[10]. Once the reactivity of the catalyst reached steady state, typically ~24 h, the temperature and intensity were varied and the effluent composition was measured by mass spectrometry (Extorr XT200) and gas chromatography (Varian CP 3800). The illumination source was a Dolan-Jenner Fiber-Lite 180 halogen light. The intensity was varied by manipulating the source power and calibrated using a combination of a ultraviolet powermeter, calibrated to 365 nm, and a CCD (Avantes AvaSpec-2048). Isotopic labelling experiments were executed using 99% O₂¹⁸ (Sigma Aldrich 602892).

DFT calculations. Density functional theory calculations were performed using a real-space grid-based implementation with the projector-augmented wave method in GPAW (ref. 48). A revised Perdew–Burke–Ernzerhof functional was used to approximate the exchange-correlation interactions[49]. The Ag(100) surface was modelled by a $2 \times 2 \times 3$ slab with 10 Å of vacuum space using 18 irreducible k-points and a grid spacing of 0.2 Å. The oxygen molecule was adsorbed parallel to the Ag–Ag bridge, which was found to be the most stable adsorption configuration on Ag(100) at 1/4 ML coverage[50]. The O₂ adsorbate and top two layers of the slab were allowed to relax until the forces on all atoms had converged to less than 0.05 eV Å⁻¹. A finite-temperature Fermi function ($k_B T = 0.1$ eV) is used to facilitate the self-consistent field convergence by smearing the band occupation around the Fermi level, and the total energy of the system is extrapolated back to $k_B T = 0$ eV. The vibrational frequency of O₂ on Ag(100) was calculated from a finite-difference approximation of the Hessian matrix. The transition state of O₂ dissociation was identified using a climbing nudged elastic band algorithm. The energy of the TNI state of O₂ on Ag(100) trapping an excited electron at the $2\pi^*$ orbital from the Fermi level is calculated using the linear-expansion Delta Self-Consistent Field (ΔSCF-DFT) method implemented in GPAW as described in Supplementary Information.

References

1. Fujishima, A. & Honda, K. Electrochemical photolysis of water at a semiconductor electrode. *Nature* **238,** 37–38 (1972).
2. Linsebiger, A. L., Lu, G. & Yates, J. T. Photocatalysis on TiO₂ surfaces: Principles, mechanisms, and selected results. *Chem. Rev.* **95,** 735–758 (1995).
3. Kudo, A. & Miseki, Y. Heterogeneous photocatalyst materials for water splitting. *Chem. Soc. Rev.* **38,** 253–278 (2009).
4. Asahi, R., Morikawa, T., Aoki, K. & Taga, Y. Visible-light photocatalysis in nitrogen-doped titanium oxides. *Science* **293,** 269–271 (2001).
5. Hou, Y. *et al.* Bioinspired molecular co-catalysts bonded to a silicon photocathode for solar hydrogen evolution. *Nature Mater.* **10,** 434–438 (2011).
6. Christopher, P., Ingram, D. B. & Linic, S. Enhancing photochemical activity of semiconductor nanoparticles with optically active Ag nanostructures: Photochemistry mediated by Ag surface plasmons. *J. Phys. Chem. C* **114,** 9173–9177 (2010).
7. Ingram, D. B. & Linic, S. Water splitting on composite plasmonic-meta/semiconductor photoelectrodes: Evidence for selective plasmon-induced formation of charge carriers near the semiconductor surface. *J. Am. Chem. Soc.* **133,** 5202–5205 (2011).
8. Mallouk, T. E. The emerging technology of solar fuels. *J. Phys. Chem. Lett.* **1,** 2738–2739 (2010).
9. Linic, S., Christopher, P. & Ingram, D. B. Plasmonic-metal nanostructures for efficient conversion of solar to chemical energy. *Nature Mater.* **10,** 911–921 (2011).
10. Christopher, P., Xin, H. & Linic, S. Visible light enhanced catalytic oxidation reactions on plasmonic Ag nanostructures. *Nature Chem.* **3,** 467–472 (2011).
11. Busch, D. G. & Ho, W. Direct observation of the crossover from single to multiple excitations in femtosecond surface photochemistry. *Phys. Rev. Lett.* **77,** 1338–1341 (1996).
12. Thompson, T. L. & Yates, J. T. Jr Monitoring hole trapping in photoexcited TiO₂(110) using a surface photoreaction. *J. Phys. Chem B* **109,** 18230–18236 (2010).
13. Westrich, T. A., Dahlberg, K. A., Kaviany, M. & Schwank, J. W. High-temperature photocatalytic ethylene oxidation over TiO₂. *J. Phys. Chem. C* **115,** 16537–16543 (2011).
14. Linic, S. & Barteau, M. A. Control of ethylene epoxidation selectivity by surface oxametallacycles. *J. Am. Chem. Soc.* **125,** 4034–4035 (2003).
15. Brus, L. Noble metal nanocrystals: Plasmon electron transfer photochemistry and single-molecule Raman spectroscopy. *Acc. Chem. Res.* **41,** 1742–1749 (2008).
16. El-Sayed, M. A. Some Interesting properties of metals confined in time and nanometer space of different shapes. *Acc. Chem. Res.* **34,** 257–264 (2001).
17. Kelly, K. L., Coronado, E., Zhao, L. L. & Schatz, G. C. The optical properties of metal nanoparticles: The influence of size, shape, and dielectric environment. *J. Phys. Chem. B* **107,** 668–677 (2003).
18. Gunnarsson, L. *et al.* Confined plasmons in nanofabricated single silver particle pairs: Experimental observations of strong interparticle interactions. *J. Phys. Chem. B* **109,** 1079–1087 (2005).
19. Kamat, P. V. Photophysical, photochemical and photocatalytic aspects of metal nanoparticles. *J. Phys. Chem. B* **106,** 7729–7744 (2002).
20. Jain, P. K., Huang, X., El-Sayed, I. H. & El-Sayed, M. A. Noble metals on the nanoscale: Optical and photothermal properties and some applications in imaging, sensing, biology, and medicine. *Acc. Chem. Res.* **41,** 1578–1586 (2008).
21. Nie, S. & Emory, S. R. Probing single molecules and single nanoparticles by surface-enhanced Raman scattering. *Science* **275,** 1102–1106 (1997).
22. Kühn, S., Håkanson, U., Rogobete, L. & Sandoghdar, V. Enhancement of single-molecule fluorescence using a gold nanoparticle as an optical nanoantenna. *Phys. Rev. Lett.* **97,** 017402 (2006).
23. Moskovits, M. Surface-enhanced Raman spectroscopy: A brief retrospective. *J. Raman Spectrosc.* **36,** 485–496 (2005).
24. Monnier, J. R., Medlin, J. W. & Barteau, M. A. Use of oxygen-18 to determine kinetics of butadiene epoxidation over Cs-promoted, Ag catalysts. *J. Catal.* **203,** 362–368 (2001).
25. Bonn, M. *et al.* Phonon-versus electron-mediated desorption and oxidation of CO on Ru(0001). *Science* **285,** 1042–1045 (1999).
26. Hatch, S. R., Zhu, X-Y., White, J. M. & Campion, A. Photoinduced pathways to dissociation and desorption of dioxygen on Ag(110) and Pt(111). *J. Phys. Chem.* **95,** 1759–1768 (1991).
27. So, S. K., Franchy, R. & Ho, W. Photodesorption of NO from Ag(111) and Cu(111). *J. Chem. Phys.* **95,** 1385–1399 (1991).
28. Dai, H-L. & Ho, W. *Laser Spectroscopy and Photochemistry on Metal Surfaces* (World Scientific, 1995).
29. Gadzuk, J. W. Hot-electron femtochemistry at surfaces: On the role of multiple electron processes in desorption. *Chem. Phys.* **251,** 87–97 (2000).
30. Mulugeta, D., Kim, K. H., Watanabe, K., Menzel, D. & Freund, H-J. Size effects in thermal and photochemistry of (NO)₂ on Ag nanoparticles. *Phys. Rev. Lett.* **101,** 146103 (2008).
31. Kim, K. H., Watanabe, K., Mulugeta, D., Freund, H-J. & Menzel, D. Enhanced photoinduced desorption from metal nanoparticles by photoexcitation of confined hot electrons using femtosecond laser pulses. *Phys. Rev. Lett.* **107,** 047401 (2011).
32. Beckerle, J. D. *et al.* Ultrafast infrared response of adsorbates on metal surfaces: Vibrational lifetime of CO/Pt(111). *Phys. Rev. Lett.* **64,** 2090–2093 (1990).

33. Bartels, L. *et al.* Dynamics of electron-induced manipulation of individual CO molecules on Cu(111). *Phys. Rev. Lett.* **80,** 2004–2007 (1998).
34. Olsen, T., Gavnholt, J. & Schiøtz, J. Hot-electron-mediated desorption rates calculated from excited-state potential energy surfaces. *Phys. Rev. B* **79,** 035403 (2009).
35. Gavnholt, J., Olsen, T., Engelund, M. & Schiøtz, J. Δ Self-consistent field method to obtain potential energy surfaces of excited molecules on surfaces. *Phys. Rev. B* **78,** 075441 (2008).
36. Wingreen, N. S., Jacobsen, K. W. & Wilkins, J. W. Inelastic scattering in resonant tunneling. *Phys. Rev. B* **40,** 11834–11850 (1989).
37. Ho, W. Reactions at metal surfaces induced by femtosecond lasers, tunneling electrons and heating. *J. Phys. Chem.* **100,** 13050–13060 (1996).
38. Olsen, T. & Schiøtz, J. Origin of power laws doe reactions at metal surfaces mediated by hot electrons. *Phys. Rev. Lett.* **103,** 238301 (2009).
39. Madey, T. E., Yates, J. T., King, D. A. & Uhlaner, C. J. Isotope effect in electron stimulated desorption: Oxygen chemisorbed on tungsten. *J. Chem. Phys.* **52,** 5215–5220 (1970).
40. Grillet, N. *et al.* Plasmon coupling in silver nanocube dimers: Resonance splitting induced by edge rounding. *ACS Nano.* **5,** 9450–9462 (2011).
41. Persson, B. N. J. On the theory of surface-enhanced Raman spectroscopy. *Chem. Phys. Lett.* **82,** 561–565 (1981).
42. Michaels, A. M., Jiang, J. & Brus, L. Ag nanocrystal junctions as the site for surface-enhanced Raman scattering of single rhodamine 6G molecules. *J. Phys. Chem. B* **104,** 11965–11971 (2000).
43. Watanabe, K., Menzel, D., Nilius, N. & Freund, H. J. Photochemistry on metal nanoparticles. *Chem. Rev.* **106,** 4301–4320 (2006).
44. Kim, K. H. *et al.* Enhanced photoinduced desorption from metal nanoparticles by photoexcitation of confined hot electrons using femtosecond laser pulses. *Phys. Rev. Lett.* **107,** 047401 (2011).
45. Kawazoe, T. *et al.* Nonadiabatic photodissociation process using an optical near field. *J. Chem. Phys.* **122,** 024715 (2005).
46. Christopher, P. & Linic, S. Shape- and size-specific chemistry of Ag nanostructures in catalytic ethylene epoxidation. *Chem. Catal. Chem.* **2,** 78–83 (2010).
47. Christopher, P. & Linic, S. Engineering selectivity in heterogeneous catalysis: Ag nanowires as selective ethylene epoxiation catalysts. *J. Am. Chem. Soc.* **130,** 11264–11265 (2008).
48. Enkovaara, J. *et al.* Electronic structure calculations with GPAW: A real-space implementation of the projector augmented wave method. *J. Phys. Condens. Matter* **22,** 253202 (2010).
49. Hammer, B., Hansen, L. & Nørskov, J. Improved adsorption energetics within density-functional theory using revised Perdew-Burke-Ernzerhof functionals. *Phys. Rev. B* **59,** 7413–7421 (1999).
50. Buatier de Mongeot, F., Cupolillo, A., Valbusa, U. & Rocca, M. Anharmonicity of the O_2-Ag(001) chemisorption. *J. Chem. Phys.* **106,** 9297–9304 (1997).

Acknowledgements

Author contributions

P.C., H.X., and S.L. developed the project and analysed the results. P.C. carried out experimental work. H.X. performed the DFT simulations. A.M. assisted with analysis. S.L. is the PhD adviser of P.C., H.X. and A.M.

Additional information

Supplementary information is available in the online version of the paper. Reprints and permissions information is available online at www.nature.com/reprints. Correspondence and requests for materials should be addressed to S.L.

Competing financial interests

The authors declare no competing financial interests.